Symmetry breaking at the (111) interfaces of $SrTiO_3$ hosting a 2D-electron system

G. M. De Luca[1,2], R. Di Capua[1,2], E. Di Gennaro[1,2], A. Sambri[1, 2], F. Miletto Granozio[2], G. Ghiringhelli[3, 4], D. Betto[5], C. Piamonteze[6], N.B. Brookes[5] and M. Salluzzo[2]

[1]*Dipartimento di Fisica, Università "Federico II" di Napoli, Complesso Monte Sant'Angelo via Cinthia, I-80126 Napoli, Italy*

[2]*CNR-SPIN, Complesso Monte Sant'Angelo via Cinthia, I-80126 Napoli, Italy*

[3] *Dipartimento di Fisica, Politecnico di Milano, Piazza Leonardo da Vinci 32, I-20133 Milano, Italy*

[4] *CNR-SPIN, Politecnico di Milano, Piazza Leonardo da Vinci 32, I-20133 Milano, Italy*

[5] *ESRF, 71 Avenue des Martyrs, 38000 Grenoble, France*

[6] *Swiss Light Source, Paul Scherrer Institut, CH-5232 Villigen PSI, Switzerland*

(Dated: June 27, 2018)

We used x-ray absorption spectroscopy to study the orbital symmetry and the energy band splitting of (111) $LaAlO_3/SrTiO_3$ and $LaAlO_3/EuTiO_3/SrTiO_3$ heterostructures, hosting a quasi two-dimensional electron system (q2DES), and of a Ti-terminated (111) $SrTiO_3$ single crystal, also known to form a q2DES at its surface. We demonstrate that the bulk tetragonal Ti-3d D_{4h} crystal field is turned into trigonal D_{3d} crystal field in all cases. The symmetry adapted a_{1g} and e^{π}_g orbitals are non-degenerate in energy and their splitting, Δ, is positive at the bare STO surface but negative in the heterostructures, where the a_{1g} orbital is lowest in energy. These results demonstrate that the interfacial symmetry breaking induced by epitaxial engineering of oxide interfaces has a dramatic effect on their electronic properties, and it can be used to manipulate the ground state of the q2DES.

Keywords: 2DEG, STM, STS, LAO/STO, interfaces, PLD

Transition metal oxides are renowed for the novel physical phenomena emerging at their surfaces and interfaces, like the formation of a quasi-two-dimensional electron system (q2DES) at the interface between (001) [1], (110) and (111) [2] $SrTiO_3$ (STO) single crystals and $LaAlO_3$ thin films (LAO). Some of the distinctive properties of the (001) LAO/STO q2DES arise from the occurrence of an orbital reconstruction, firstly demonstrated by x-ray linear dichroism (XLD) [3] and later on by Angle Resolved Photoemission Spectroscopy (ARPES).[4, 5, 6, 7] In the (001) LAO/STO, this orbital reconstruction causes a reverse ordering and splitting of the bulk conduction bands derived from the non-degenerate t_{2g} ($3d_{xy}$, $3d_{xz}$, $3d_{yz}$) orbitals of Ti 3d-states (Fig. 1a). A similar orbital reconstruction was observed also in other (001) titanate heterostructures, like in the (001) $LaAlO_3/EuTiO_3/SrTiO_3$ (LAO/ETO/STO) system, which hosts a spin-polarized q2DES.[8, 9] In the (110) LAO/STO, instead, the q2DES does not show the reverse ordering of the bands as it happens in the the (001) cases.[10, 11] However, in both systems, the bulk tetragonal crystal field, D_{4h}, associated to the characteristic distorted octahedral oxygen-cages around Ti-ions, is retained also at the interface. Thus, the overall q2DES's electronic properties can still be described within a D_{4h} frameworks.

The D_{4h} symmetry is on the other hand naturally broken at the (111) $SrTiO_3$ surface, where the crystal field becomes trigonal owing to the D_{3d} symmetry associated to the hexagonal surface lattice.[12] Within the D_{3d} symmetry, the t_{2g} states are mixed, so that the three usual orbitals transform into a_{1g} and e^{π}_g states (Fig. 1b), which are futher split by the crystal field and/or by the spin-orbit coupling.[13] Consequently, the band structure of (111) oxide heterostructures is susceptible of being more significantly altered at their interfaces respect the (001) and (110) cases.

As matter of fact, interesting phenomena were theoretically predicted in (111) oxides, like non-trivial topological effects and the possibility of quantum Hall effect up to room temperature .[14] In particular, a massive symmetry breaking was predicted in the case of (111) LAO/STO quantum wells, with ordering of the (a_{1g}, e^{π}_g) derived bands depending on the strain and on the confinement.[12]

ARPES studies of the (111) STO surface state showed a Fermi surface interpreted as originating from the projection on the (111) plane of the confined and degenerate $3d_{xz}$, $3d_{yz}$, and $3d_{xy}$.[15, 16] Since the surface unit cell of (111) STO has an inherent trigonal symmetry, the derived surface states have to be described as a combination of t_{2g} orbitals, thus in

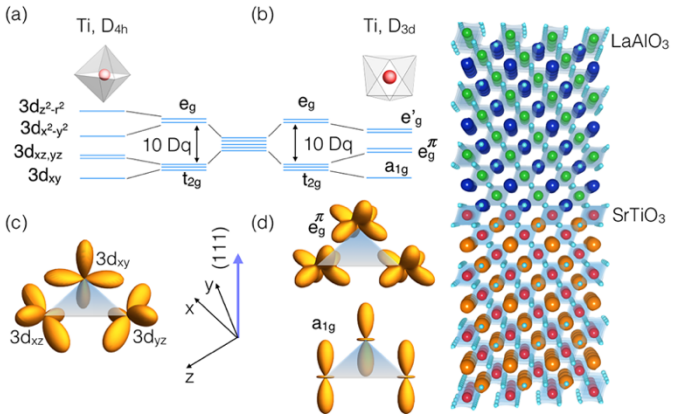

Fig. 1: Energy diagram of the 3d Ti states in the case of (a) tetragonal and (b) trigonal crystal fields. (c) t_{2g} $3d_{xy}$, $3d_{xz}$, $3d_{yz}$ orbitals and (d) a_{1g} and e^{π}_{g} orbitals viewed from the (111) surface (shaded triangles). On the right a schematic of the (111) LAO/STO heterostructure.

terms of a_{1g} or e^{π}_{g} derived bands. One would then expect a band structure very different from the bulk. Consequently, it is natural to ask ourselves if the orbital and the electronic symmetry of the Ti 3d-bands in (111) heterostructures and at the (111) STO surface are perturbed by surface/interface symmetry breaking, and how this would affect the global properties of the q2DES formed thereby.

Here we have determined the orbital symmetry and splitting of the Ti-3d states at the (111) STO surface and at the (111) LAO/STO and LAO/ETO/STO interfaces by measuring, in total electron yield (TEY), the x-ray absorption spectra (XAS) and related x-ray linear dichroism (XLD). The TEY XAS and XLD spectra probe the interface electronic properties within a depth of about 3 nm from the interface. In all the (111) heterostructures we find that a D_{3d} symmetry replaces the tetragonal D_{4h} symmetry of bulk $SrTiO_3$. Moreover, the a_{1g} and e^{π}_{g} orbitals are non-degenerate, and their splitting depends sensitively on the specific system analyzed, so that it is opposite in sign in the heterostructures compared to the bare (111) STO surface state.

The XAS measurements were performed at the ID32 beamline of the European Synchrotron Radiation Facility (ESRF) [17] and at the X-treme beamline of the Swiss Light Source (SLS) [18]. In both cases, the samples were measured in a variable temperature cryostat in ultra-high vacuum. Ti-terminated (111) STO single crystals were prepared by BHF etching and oxygen annealing, and were characterized by a 1x1 surface lattice. The LAO/STO and LAO/ETO/STO heterostructures were grown by pulsed laser deposition assisted by reflection high energy electron diffraction [19, 20] onto the (111) STO single crystals mentioned above, using a background oxygen pressure of $1x10^{-4}$ mbar and laser fluence of 1.5 J/cm^2. In particular, we studied heterostructures characterized by 10 unit cells (uc) of LAO

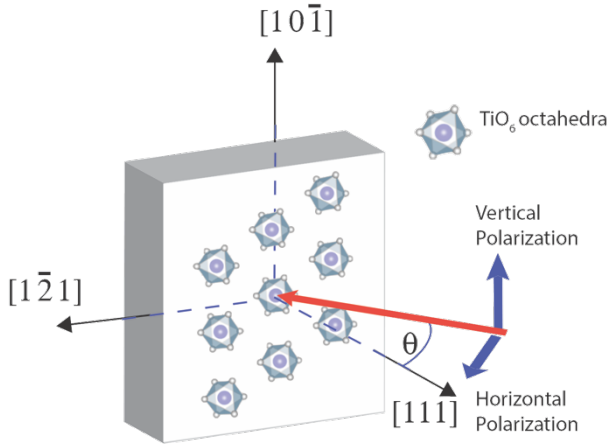

Fig. 2: Schematic of the XAS and XLD experimental configuration. The x-rays propagation vector (red arrow) forms an angle θ with the [111] surface normal. Blue lines indicate the direction of the corresponding polarization vectors. The [10$\bar{1}$] crystalline direction vector is parallel to the vertical polarization for any incidence angle. On the surface plane we have superimposed the schematic arrangement of the Ti (violes spheres) and oxygen (gray spheres).

in the case of (111) LAO/STO, and by 3 uc of ETO plus 10 uc of LAO sequentially deposited on STO in the case of (111) LAO/ETO/STO.[20] In both types of samples, we observed a metallic temperature dependence of the sheet resistance down to 4.2 K.[20] The low temperature values of the sheet resistances were comparable to standard (001) LAO/STO and LAO/ETO/STO heterostructures deposited in the same deposition conditions.

The samples were mounted on the XAS setups with the (111) surface in the vertical laboratory plane, and the vertical axis (V) parallel to the [10$\bar{1}$] crystallographic direction determined by x-ray diffraction, i.e. parallel to one of the three equivalent Ti-Ti bonds within the hexagonal surface lattice (Fig 2). The energy resolution at both beamlines was around 100 meV. X-ray linear dichroism spectra were obtained by averaging at least 16 XAS spectra for each of the two linear horizontal (H) and vertical (V) polarizations. Linear dichroism spectra were measured as function of the angle θ between the incident photons and the surface normal (Fig. 2). While for the vertical polarization the x-ray electric field is always parallel to the surface and to the [10$\bar{1}$] crystallographic direction (Fig. 2), with horizontal polarization, the electric field vector is in the (111) surface plane and along the [1$\bar{2}$1] direction for θ=0 (Normal incidence, NI), and almost parallel to the [111] lattice vector, i.e. along the surface normal, for θ =70° (Grazing incidence, GI).

The XAS and XLD experimental spectra were compared to theoretical spectra obtained by atomic multiplet scattering calculations using the CTM4XAS code. [21]

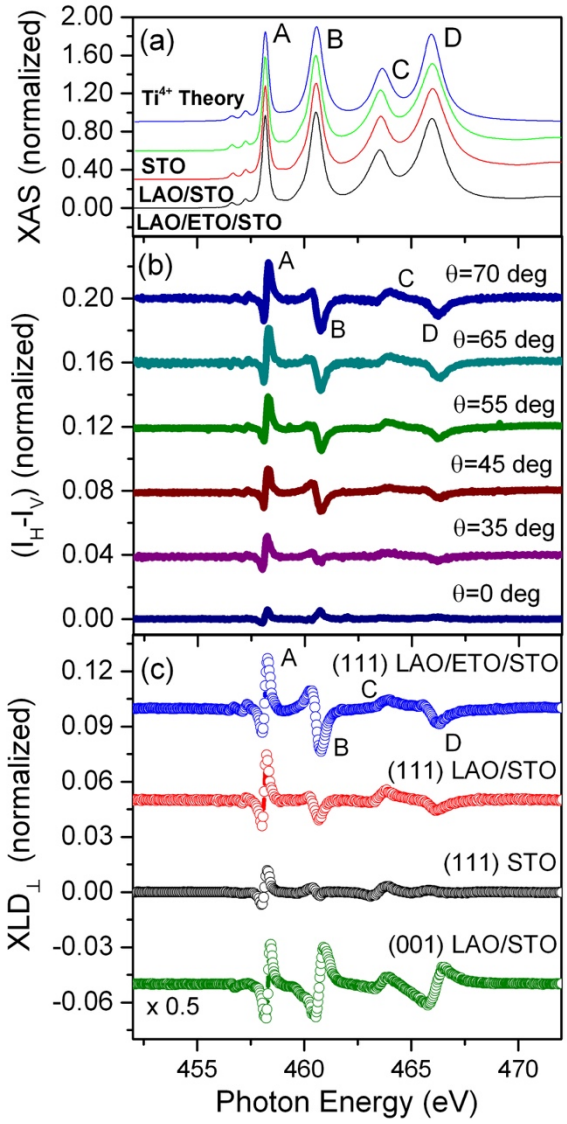

Fig. 3: Total electron Yield XAS spectra of (111) STO (green line) LAO/STO (red line) and LAO/ETO/STO (black line) measured at 5 K in grazing incidence conditions. The blue line is an atomic multiplet calculation assuming a pure Ti^{4+} valence and using the parameters listed in Table 1. (b) I_H-I_V data in the same conditions as function of the angle θ measured on the (111) LAO/ETO/STO sample. Features A, B, C and D indicate the main absorption peaks at L_3 (A, B) and L_2 (C, D). (c) $XLD_\perp$ data, normalized to the XAS maxima at L_3 edge of (001) LAO/STO (green cicles, divided by a factor 2), (111) STO (black circles), (111) LAO/STO (red circes) and (111) LAO/ETO/STO (blue circles). The data are shifted by a constant factor (0.05) for clarity.

In Fig. 3a we show a comparison between the Ti- $L_{2,3}$ edge XAS spectra of the three systems. We can see that the spectra on the three different systems analyzed are all very similar, apart a very slight increase (less than 5%) of the HWHMs of the main peaks in the case of the LAO/STO and LAO/ETO/STO heterostructures as compared to the (111) STO single crystal. The XAS spectra can be reproduced assuming a $3d^0$ atomic configuration (Ti^{4+}) using the parameters listed in Table 1, namely the value of 10Dq, i.e. the overall splitting between e_g and t_{2g} orbitals, the Slater integrals, and the Lorentzian broadenings (HWHM) of the four peaks in the XAS spectra (Fig. 3a). In Fig. 3a we used a D_{3d} symmetry, however similar XAS spectra are obtained using a D_{4h} symmetry.

Table 1: Crystal field parameters used to reproduce the XAS spectra of the heterostructures studied. HWHM is the Half Width at Half Maximum Lorentian broadenings of the different peaks.

10Dq (eV)	slater (%)	HWHM Peak A (eV)	HWHM Peak B (eV)	HWHM Peak C (eV)	HWHM Peak D (eV)
2.23	80	0.1	0.34	0.5	0.55

In Fig. 3b we show the angle dependence of the $XLD = I_H - I_V$ dichroic spectra measured at 5 K of the LAO/ETO/STO q2DES. We can see that while the XLD intensity changes as function of the angle, its shape remains substantially constant from 35° to 70°. This result suggests that the out-of-plane dichroism, which is mainly probed in gracing incidence, dominates the $I_H - I_V$ spectral shape. In normal incidence, θ =0°, on the other hand, $I_H - I_V$ is much smaller and has a different shape, since it is related to in plane linear dichroism $XLD_{||} = I_{[1\bar{2}1]} - I_{[10\bar{1}]}$.

From the spectra acquired between 35° and 70°, we can determine the experimental out-of-plane dichroism, $XLD_\perp = I_{[111]} - I_{[10\bar{1}]}$, considering that $I_{[10\bar{1}]} = I_V$ and $I_{[111]} \cong (I_H - I_V cos^2\vartheta)/sin^2\vartheta$ [22]. As shown in the suppl. mat,[20] the $XLD_\perp$ data obtained from different angles coincide, confirming that the dichroic signal is due to the in-plane/out-of plane anisotropy. Moreover, the $XLD_\perp$ spectral shape of (111) heterostructures, shown in Fig. 3c, differs significantly from that measured previously on (001) and (110) LAO/STO, and on bulk (001) STO. [3,10] In particular, the three selected cases of (111) STO heterostructures and the (001) LAO/STO $XLD_\perp$ differ both in the amplitude and in the shape of the main features (A, B, C, D).

Before comparing the data to theoretical calculations, we discuss what would be the expected $XLD_\perp$ in case of D_{4h} symmetry, i.e, in a case where the bulk symmetry of STO is preserved up to the interface/surface unit cells probed by TEY-XLD (around 3 nm). Then the $XLD_\perp$ would be a combination of the $I_{[001]}$ and $I_{[100]}$ Ti $L_{2,3}$ XAS along the [001] and [100] directions, calculated in the D_{4h} symmetry. For example, the out of plane dichroism, $XLD_{\perp,111,D4h}$, would be given by [20]:

$$XLD_{\perp,111,D4h} = I_{[111]} - I_{[10\bar{1}]} = \frac{1}{6}\left(I_{[100]} - I_{[001]}\right);$$

while the in plane $XLD_{\|,111,D4h}$ dichroism would be:

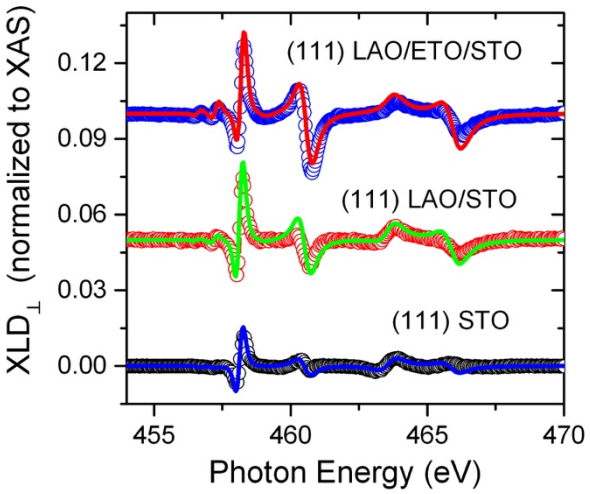

Fig. 4: Comparison between out of plane linear dichroism spectra measured in total electron yield of (111) STO (black circles), LAO/STO (red circles) and LAO/ETO/STO (blue circles. Continuous lines are the best fit of the data by atomic multiplet calculations

$$XLD_{\parallel,111,D4h} = I_{[1\bar{2}1]} - I_{[10\bar{1}]} = \frac{1}{3}\left(I_{[100]} - I_{[001]}\right)$$

Thus, if the tetragonal symmetry is preserved, with consequent degeneracy of the t_{2g} states, the dichroism would be zero also for the (111) STO surface. Moreover, even in the case of non-degenerate t_{2g} states, the non-vanishing *XLDs* would have opposite sign with respect to the $XLD_{\perp} = I_{[001]} - I_{[100]}$ of (001) heterostructures, and their shape would be similar to the one measured in the case of (110) LAO/STO. [10] The data show clearly that this is not case, thus suggesting a breaking of symmetry for all the three systems analyzed. In particular, the features B and D in the spectra have a shape reversed compared to the the (001) LAO/STO interface, while the features A and C are similar in shape. Furthermore, the overall amplitude of the dichroism is smaller in (111) heterostructures.

In order to understand the effective symmetry of the novel electronic configuration, we fit the XAS and the $XLD_{\perp}$ spectra using atomic multiplet scattering calculations by the CTM4XAS code. Starting from the XAS analysis shown in Figure 3a, we then calculate the $XLD_{\perp}$ spectra of $3d^0$ Ti^{4+} ions, in the case of a D_{3d} symmetry for various values of the a_{1g} - e^{π}_{g} splitting, depending on the crystal field terms D_{τ} and D_{σ}, the only parameters optimized in the fitting. More in details, it is possible to show that the energy splitting $\Delta = E(a_{1g}) - E(e^{\pi}_{g})$ is given by [20, 23]:

$$\Delta = \sqrt{\Gamma_{e_g}} - 5D_q - 5/2\, D_\sigma - 7/2\, D_\tau$$

with $\Gamma_{e_g} = \left(5D_q\right)^2 + (3/2\, D_\sigma)^2 + (5/2\, D_\tau)^2 - 5D_qD_\sigma + 25/3\, D_qD_\tau - 15/2\, D_\sigma D_\tau$

Table 2: D_σ and D_τ parameters obtained from atomic multiplet calculations reproducing the XLD data of Fig. 4 and the integral of the XLD normalized to the integral of the sum $I_{[111]} + I_{[10\bar{1}]}$.

Sample	D_σ (meV)	D_τ (meV)	Δ (meV)	XLD ($x10^{-3}$)
STO	2±0.3	-2.2±0.1	8±3	0.1±0.1
LAO/STO	12±1	-4.2±0.2	-8±3	-3.0±0.5
LAO/ETO/STO	16±1	-4.2±0.2	-20±3	-6.0±0.5

It turns out that peaks A and C are roughly influenced by D_{τ}, while B and D depend mainly on D_{σ}. For (111) STO the best agreement is for D_{τ} = -2.2 meV and D_{σ} = 2 meV, corresponding to Δ= +8 meV, implying that the orbitals of e^{π}_{g} symmetry are the lowest in energy. We remind that the a_{1g} orbital is an equal weight linear combination of the pristine $3d_{xz}$ $3d_{yz}$ and $3d_{xy}$ orbitals with real coefficients, while for the e^{π}_{g} the coefficients are complex numbers. Therefore, the orbital symmetry is quite different from the one expected in the case of bulk t_{2g} states simply projected on the (111) surface. The opposite case, is the one of the (111) LAO/ETO/STO (and LAO/STO) heterostructure, where we find Δ= -20 (-8) meV, i.e. the lowest energy lying orbitals have a_{1g} symmetry.

It is important to underline that from the analysis it emerges that STO-based heterostructures are characterized by an electronic configuration which is close to a perfect t_{2g}^0 ($3d^0$) occupation. However, the integral of the $XLD_{\perp}$ spectra is not null, and in particular we find it small and slightly positive in the case of the (111) STO surface, while it is more than one order of magnitude larger, and negative in sign, in the case of the heterostructures, as shown in Table 2. The negative $XLD_{\perp}$ integral suggests that the (few) 3d electrons in the (111) q2DES preferentially occupy bands derived by orbitals that have a predominant out-of-plane character, i.e. a_{1g} derived bands in both (111) LAO/STO and LAO/ETO/STO, in agreement with the overall $XLD_{\perp}$ data.

Discussion and conclusions (111) perovskite oxide heterostructures were proposed as possible candidates of quantum Hall effect systems and of non trivial topological states.[14] The important ingredients to get a topological phase in these systems are the presence of a sizable spin-orbit coupling and of a sufficiently strong trigonal crystal field that can open a gap between otherwise degenerate t_{2g} manifolds. While these theoretical predictions did not include the STO case, because titanium is close to a t_{2g}^0 occupation, it has been also shown that LAO/STO quantum wells can host a variety of unconventional ground states, ranging from spin, orbital polarized (with selective e^0_g, a_{1g}, or d_{xy} occupation), Dirac point Fermi surfaces, to charge-ordered flat band phases, as function of the strain and confinement. [12]

In this experimental work we demonstrate that some of the crucial ingredients needed to realize these phases are actually present in (111) STO-based heterostructures.

In particular, we show that we can create a q2DES with a D_{3d} orbital symmetry, as opposite to the bulk D_{4h} symmetry, in which the trigonal crystal field is sufficiently strong to open a gap up to 20 meV between a_{1g} and e^{π}_{g} states. This gap can be changed, and inverted through epitaxial engineering. Since LAO/STO based heterostructures are characterized by a sizable Rashba spin-orbit coupling in both (001) [24] and (111) cases [25], this study opens interesting perspectives for the exploration of novel unconventional ground states in (111) STO based heterostructures.

ACKNOWLEDGMENTS

The Authors acknowledge received funding from the project Quantox of QuantERA ERA-NET Cofund in Quantum Technologies (Grant Agreement N. 731473) implemented within the European Union's Horizon 2020 Programme".

REFERENCES

[1] A. Ohtomo and H. Y. Hwang, Nature **427**, 423 (2004).
[2] G. Herranz, F. Sánchez, N. Dix, M. Scigaj, and J. Fontcuberta, Sci. Rep. **2**, 758 (2012).
[3] M. Salluzzo, et al., Phys. Rev. Lett. **102**, 166804 (2009).
[4] A. F. Santander-Syro, et al. Nature **469**, 189 (2011).
[5] W. Meevasana, et al., Nature Materials **10**, 114 (2011).
[6] G. Berner, et al. Phys. Rev. Lett. **110**, 247601 (2013)
[7] C. Cancellieri, et al., Phys. Rev. B **89**, 121412 (2014).
[8] G. M. De Luca, et al., Phys. Rev. B **89**, 224413 (2014).
[9] D. Stornaiuolo, et al., Nature Materials **15**, 278 (2015).
[10] D. Pesquera, et al. , Phys. Rev. Lett. **113**, 156802 (2014).
[11] Z. Wang, et al., Proceedings of the National Academy of Sciences **111**, 3933 (2014).
[12] D. Doennig, W. E. Pickett, and R. Pentcheva, Phys. Rev. Lett. **111**, 126804 (2013).
[13] Daniel I. Khomskii, Transition Metal Compounds, Cambridge University Press 978-1-107-02017-7 (2014). See Chapter 3.
[14] Di Xiao, W. Zhu, Y. Ran, N. Nagaosa, and S. Okamoto, Nature Communications **2**, 596 (2011).
[15] S. McKeown Walker, et al., Phys. Rev. Lett. **113**, 177601 (2014).
[16] T. C. Rödel, et al., Phys. Rev. Applied **1**, 051002 (2014).
[17] K. Kummer, et al., J. Synchrotron Rad. **23**, 464 (2016).
[18] C. Piamonteze, et al., J. Synchrotron Radiat. **19**, 661 (2012).
[19] P. Perna, et al., Appl. Phys. Lett. **97**, 152111 (2010).
[20] see suppl. materials.
[21] E. Stavitski and F. M. F. de Groot, Micron **41**, 687 (2010).
[22] In the formula we have considered that $I_{(10\bar{1})} \cong I_{(1\bar{2}1)}$ since the NI linear dichroism is very small.
[23] M. Haverkort, PhD thesis, Universität Koeln. (2005); arXiv: cond mat/0505214v1
[24] A. D. Caviglia, M. Gabay, S. Gariglio, N. Reyren, C. Cancellieri, and J. M. Triscone, Phys. Rev. Lett. **104**, 126803 (2010).
[25] P. K. Rout, E. Maniv, and Y. Dagan, Phys. Rev. Lett. **119**, 237002 (2017).

Supplementary Material

Symmetry breaking at the (111) interfaces of $SrTiO_3$ hosting a 2D-electron system

G. M. De Luca[1,2], R. Di Capua[1,2], E. Di Gennaro[1,2], A. Sambri[1, 2], F. Miletto Granozio[2], G. Ghiringhelli[3, 4], D. Betto[5], C. Piamonteze[6], N.B. Brookes[5] and M. Salluzzo[2]

[1]*Dipartimento di Fisica, Università "Federico II" di Napoli, Complesso Monte Sant'Angelo via Cinthia, I-80126 Napoli, Italy*

[2]*CNR-SPIN, Complesso Monte Sant'Angelo via Cinthia, I-80126 Napoli, Italy*

[3] *Dipartimento di Fisica, Politecnico di Milano, Piazza Leonardo da Vinci 32, I-20133 Milano, Italy*

[4] *CNR-SPIN, Politecnico di Milano, Piazza Leonardo da Vinci 32, I-20133 Milano, Italy*

[5] *ESRF, 71 Avenue des Martyrs, 38000 Grenoble, France*

[6] *Swiss Light Source, Paul Scherrer Institut, CH-5232 Villigen PSI, Switzerland*

(Dated: June 27, 2018)

Supplementary Note 1

In the D_{4h} symmetry, in the simple ortho-normal base *[100]*, *[010]*, *[001]*, the angle α_{hk} between two vectors $\boldsymbol{h}$ and $\boldsymbol{k}$ characterized by indices $[h_x, h_y, h_z]$ and $[k_x, k_y, k_z]$ respectively, satisfies the relation (from $\boldsymbol{h}\cdot\boldsymbol{k} = |\boldsymbol{h}||\boldsymbol{k}|\cos\alpha_{hk}$):

$$\cos^2 \alpha_{hk} = \frac{\left(h_x k_x + h_y k_y + h_z k_z\right)^2}{\left(h_x^2 + h_y^2 + h_z^2\right)\left(k_x^2 + k_y^2 + k_z^2\right)} \tag{S1}$$

Therefore, the XAS intensity along a generic direction $\boldsymbol{n} = (n_x, n_y, n_z)$ can be written as:

$$I_{nx,\, ny,\, nz} = I_{[1,0,0]} \cos^2\alpha_x + I_{[0,1,0]} \cos^2\alpha_y + I_{[0,0,1]} \cos^2\alpha_z \tag{S2}$$

where α_x, α_y, α_z, are the angles formed by $\boldsymbol{n}$ and the base vectors, and:

$$\cos^2 \alpha_j = \frac{n_j^2}{n_x^2 + n_y^2 + n_z^2} \tag{S3}$$

If the bulk symmetry of STO were preserved up to the interface/surface, it should happen that $I_{[1,0,0]} = I_{[0,1,0]} \neq I_{[0,0,1]}$, and therefore we could write:

$$XLD_{\perp,111,D4h} = I_{[111]} - I_{[10\bar{1}]} = \frac{1}{3}\left(I_{[100]} + I_{[010]} + I_{[001]}\right) - \frac{1}{2}\left(I_{[100]} + I_{[001]}\right) = \\ = -\frac{1}{6}I_{[100]} + \frac{1}{3}I_{[010]} - \frac{1}{6}I_{[001]} = \frac{1}{6}\left(I_{[100]} - I_{[001]}\right) \quad \text{(S4)}$$

$$XLD_{\parallel,111,D4h} = I_{[\bar{1}2\bar{1}]} - I_{[10\bar{1}]} = \frac{1}{6}I_{[100]} + \frac{2}{3}I_{[010]} + \frac{1}{6}I_{[001]} - \frac{1}{2}\left(I_{[100]} + I_{[001]}\right) = \\ = -\frac{1}{3}I_{[100]} + \frac{2}{3}I_{[010]} - \frac{1}{3}I_{[001]} = \frac{1}{3}\left(I_{[100]} - I_{[001]}\right) \quad \text{(S5)}$$

In our experimental setup, the direction of Linear Vertical (LV) polarization of the incident light is always parallel to the $[10\bar{1}]$ crystallographic direction, independently on the angle θ between the normal to the sample surface (i.e., the $[111]$ crystallographic direction) and the propagation vector of the incident light. On the contrary, the direction of Linear Horizontal (LH) polarization of the incident light forms an angle θ with the $[1\bar{2}1]$ crystallographic direction, lying in the $[1\bar{2}1]$-$[111]$ plane (cfr. Fig. S1).

As a consequence:

$$\begin{cases} I_V = I_{[10\bar{1}]} & \forall\theta \\ I_H = I_{[\bar{1}2\bar{1}]}\cos^2\theta + I_{[111]}\sin^2\theta \end{cases} \Rightarrow I_V - I_H = I_{[10\bar{1}]} - \left(I_{[\bar{1}2\bar{1}]}\cos^2\theta + I_{[111]}\sin^2\theta\right) \quad \text{(S6)}$$

Being $XLD_\perp = I_{[111]} - I_{[10\bar{1}]}$ and $XLD_\parallel = I_{[\bar{1}2\bar{1}]} - I_{[10\bar{1}]}$, from relations (S6) it easily comes out that:

$$I_H - I_V = XLD_\parallel \cos^2\theta + XLD_\perp \sin^2\theta \quad \text{(S7)}$$

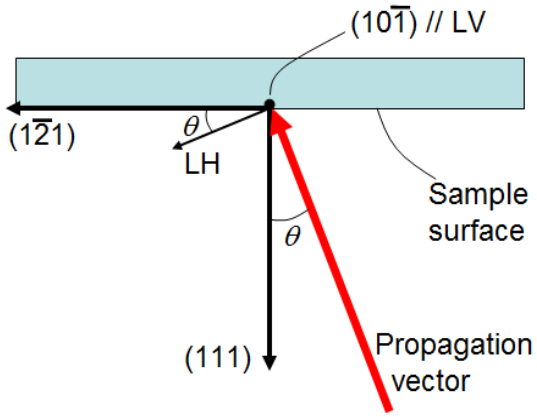

Fig. S1: a sketch illustrating the relation between the LH polarization and the crystallographic direction as a function of the angle q between the propagation vector of light and the normal to the sample surface.

In Normal Incidence ($\theta = 0$), (S7) gives $I_H - I_V = XLD_\parallel$, as expected. On the other hand, for $\theta = 90°$, from (S7) we would have $I_H - I_V = XLD_\perp$. At θ = 70° (Grazing Incidence condition in our experiment) we can compute from

(S7): $I_H - I_V = 0.883\ XLD_\perp + 0.117\ XLD_\parallel$, which means, as stated in the main text, that at Grazing Incidence we mainly probe the out-of-plane dichroism.

In addition, from (S7) we can infer:

$$XLD_\perp = \frac{I_H - I_V}{\sin^2\theta} - XLD_\parallel \tan^2\theta \qquad \text{(S8)}$$

which can be approximated at $(I_H - I_V)/\sin^2\theta$, being in-plane XLD much smaller than out-of-plane XLD.

In Fig. S2 we show $XLD_\perp$ for LAO/ETO/STO (111) heterostructure determined from the measured I_H-I_V. It is possible to note that the result is very similar for each value of θ from 35° to 70°.

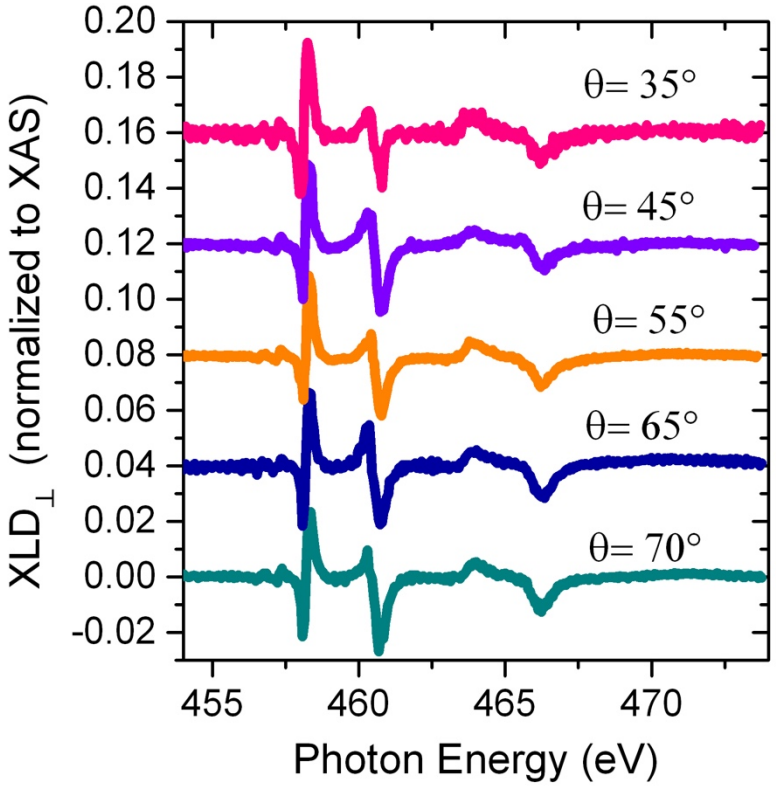

Fig. S2: Out of plane dichoism normalized to the XAS intensity at L_3, of the (111) LAO/ETO/STO heterostructure determined from the measured dichroism at different angles θ from 35° (top) to 70° (bottom). The data are displaced by a constant factor 0.04.

Supplementary Data: sample properties and characterizations

From the RHEED images (Figs. S3a and S3b) of bare (111) STO and of a 10 unit cells LAO film deposited on STO (111), we can see that the structural quality of the sample is preserved also after the deposition and that the surface lattice is not reconstructed in both cases. In Fig. S3c we show the temperature dependences of the sheet resistance of (111) LAO/ETO/STO and LAO/STO heterostructures, which are very similar to the typical data measured on (001) heterostructures.

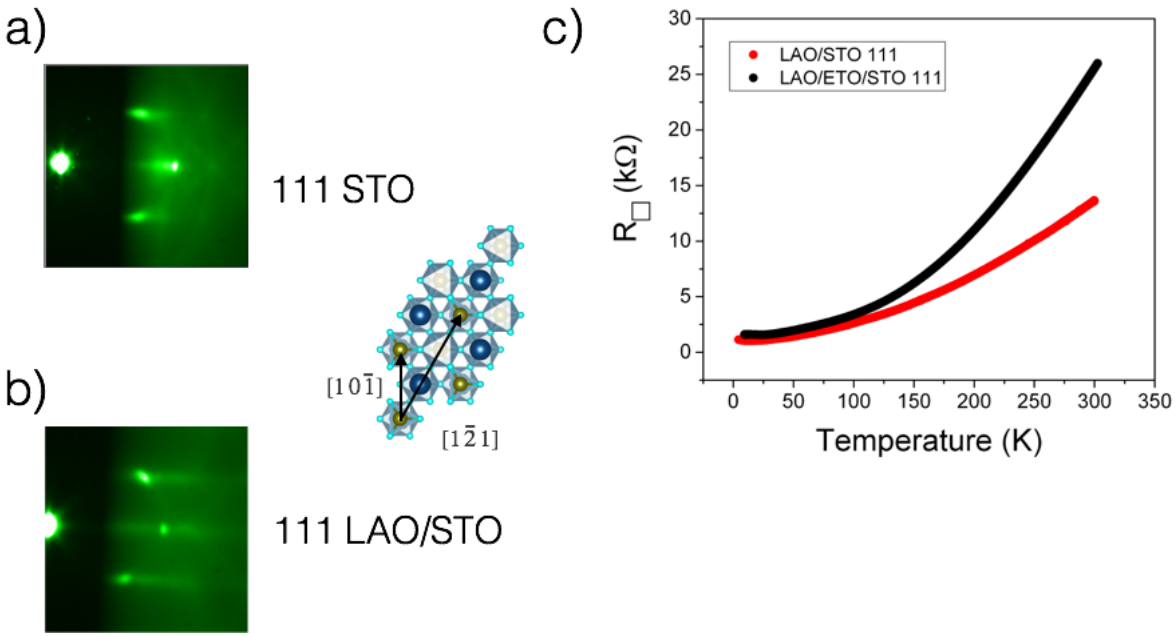

Fig. S3: RHEED image along the $[10\bar{1}]$ crystallographic direction for (a) (111) STO and (b) (111) LAO/STO sample. (c) Sheet resistance of (111) LAO/STO (red circles) and (111) LAO/ETO/STO (black circles) as a function of the temperature.

Supplementary note 2: Calculation of the XAS and XLD spectra using a trigonal crystal field

If we quantize the orbitals along the (111) direction, *i.e.* the *z* axis is directed along (111), we have the following orbitals:

$$\begin{aligned} a_{1g} &= d_0 \\ e_g^{\pi\pm} &= \sqrt{\frac{2}{3}}d_{\pm2} \mp \sqrt{\frac{1}{3}}d_{\mp1} \\ e_g'^{\pm} &= \sqrt{\frac{1}{3}}d_{\pm2} \pm \sqrt{\frac{2}{3}}d_{\mp1} \end{aligned} \tag{S9}$$

where d_{ml} are the spherical harmonics Y_2^{ml} quantized along the (111) direction.

Using this convention, we have, for trigonal crystal field V_t:

$$\begin{aligned} \langle d_{\pm2}|V_t|d_{\pm2}\rangle &= -\frac{2}{3}Dq + 2D_\sigma - D_\tau \\ \langle d_{\pm1}|V_t|d_{\pm1}\rangle &= -\frac{8}{3}Dq - D_\sigma + 4D_\tau \\ \langle d_0|V_t|d_0\rangle &= -4Dq - 2D_\sigma - 6D_\tau \\ \langle d_{\pm2}|V_t|d_{\mp1}\rangle &= \langle d_{\mp1}|V_t|d_{\pm2}\rangle = \pm\frac{10}{3}\sqrt{(2)}Dq \end{aligned} \tag{S10}$$

Therefore, we have:

$$\begin{aligned} \langle a_{1g}|V_t|a_{1g}\rangle &= -4Dq - 2D_\sigma - 6D_\tau \\ \langle e_g^{\pi\pm}|V_t|e_g^{\pi\pm}\rangle &= -4Dq + D_\sigma + \frac{2}{3}D_\tau \\ \langle e_g'^{\pm}|V_t|e_g'^{\pm}\rangle &= 6Dq + \frac{7}{3}D_\tau \\ \langle e_g^{\pi\pm}|V_t|e_g'^{\pm}\rangle &= \sqrt{2}D_\sigma - \frac{5\sqrt{2}}{3}D_\tau \end{aligned} \tag{S11}$$

The orbitals are not eigenfunctions of the system anymore. As you can see, there is a non-diagonal matrix element that mixes the two types of e_g orbitals (obviously). The a_{1g} stands alone and it is an eigenfunction.

To be accurate one should diagonalise the Hamiltonian for the e_g states and find eigenfunctions and eigenvalues.

Hamiltonian:

$$\begin{array}{c} \\ e_g^\pi \\ e_g' \end{array} \begin{array}{c} \begin{array}{cc} e_g^\pi & e_g' \end{array} \\ \begin{bmatrix} -4Dq + D_\sigma + \frac{2}{3}D_\tau & \sqrt{2}Dq - \frac{5\sqrt{2}}{3}D_\tau \\ \sqrt{2}Dq - \frac{5\sqrt{2}}{3}D_\tau & 6Dq + \frac{7}{3}D_\tau \end{bmatrix} \end{array} \tag{S12}$$

Eigenvalues:

$$\begin{aligned} E_1 &= \frac{1}{6}\left(6Dq + 3D_\sigma + 9D_\tau - \sqrt{3}\sqrt{300Dq^2 - 60DqD_\sigma + 100DqD_\tau + 27D_\sigma^2 - 90D_\sigma D_\tau + 75D_\tau^2}\right) \\ &= Dq + \frac{1}{2}D_\sigma + \frac{3}{2}D_\tau - \sqrt{\Gamma_{e_g}} \\ E_2 &= \frac{1}{6}\left(6Dq + 3D_\sigma + 9D_\tau + \sqrt{3}\sqrt{300Dq^2 - 60DqD_\sigma + 100DqD_\tau + 27D_\sigma^2 - 90D_\sigma D_\tau + 75D_\tau^2}\right) \\ &= Dq + \frac{1}{2}D_\sigma + \frac{3}{2}D_\tau + \sqrt{\Gamma_{e_g}} \end{aligned} \tag{S13}$$

with

$$\Gamma_{e_g} = 25Dq^2 + \frac{9}{4}D_\sigma^2 + \frac{25}{4}D_\tau^2 - 5DqD_\sigma + \frac{25}{3}DqD_\tau - \frac{15}{2}DqD_\tau \tag{S14}$$

Eigenvectors in base $e_g^\pi, e_g^{/}$:

$$\begin{aligned}
\Phi_1 &= \left\{ \frac{-\sqrt{3}\sqrt{300Dq^2 - 60DqD_\sigma + 100DqD_\tau + 27D_\sigma^2 - 90D_\sigma D_\tau + 75D_\tau^2} - 30Dq + 3D_\sigma - 5D_\tau}{2\sqrt{2}(3D_\sigma - 5D_\tau)}, 1 \right\} \\
&= \left\{ \frac{-6\sqrt{\Gamma_{e_g}} - 30Dq + 3D_\sigma - 5D_\tau}{2\sqrt{2}(3D_\sigma - 5D_\tau)}, 1 \right\} \\
\Phi_2 &= \left\{ \frac{+\sqrt{3}\sqrt{300Dq^2 - 60DqD_\sigma + 100DqD_\tau + 27D_\sigma^2 - 90D_\sigma D_\tau + 75D_\tau^2} - 30Dq + 3D_\sigma - 5D_\tau}{2\sqrt{2}(3D_\sigma - 5D_\tau)}, 1 \right\} \\
&= \left\{ \frac{+6\sqrt{\Gamma_{e_g}} - 30Dq + 3D_\sigma - 5D_\tau}{2\sqrt{2}(3D_\sigma - 5D_\tau)}, 1 \right\}
\end{aligned} \tag{S15}$$